

# Modeling and Control of Mid-flight Coupling of Quadrotors: A new concept for Quadrotor cooperation

Daniel T. Larsson, Chuong H. Nguyen and Panagiotis Artemiadis\*, *Senior Member, IEEE*

**Abstract**—Multirotor vehicles, quadrotors specifically, have formed a fast-growing field in robotics, with the range of applications spanning from surveillance and reconnaissance to agriculture and large area mapping. Although in most applications, a single quadrotor is used, there is an increasing interest in architectures controlling multiple quadrotors executing a collaborative task. This paper introduces a new concept of control involving more than one quadrotors, according to which two quadrotors can be physically coupled in mid-flight. This concept equips the quadrotors with new capabilities, e.g. increased payload or pursuit and capturing of other quadrotors. A comprehensive analysis of the approach is presented for the system of two coupled quadrotors. The dynamics and modeling of the coupled system is presented together with a discussion regarding the coupling mechanism and the overall control architecture. Controller gains were found using Linear Quadratic Control (LQR) techniques combined with Proportional Integral Derivative (PID) gain scheduling to account for the change in system dynamics to ensure stability and satisfactory response characteristics in actual experiments. Finally, the proposed methods are evaluated through an experiment that involved physical coupling and coupled flight of a pair of quadrotors.

## I. INTRODUCTION

In recent years, quadrotors have received much attention thanks to their versatility in both academic research and commercial applications. Examples of these applications are surveillance, agricultural data collection, search and rescue, crowd control, domestic security, as well as assisting in various military operations [1], [2].

Considering their popularity, much research has been done in modeling the dynamics and control of quadrotors. The scope and application of the research recently completed is also very diverse. In some cases, authors will focus attention to the dynamical details of the quadrotor in all aspects of flight; from the hover state and motor modeling to aerodynamic blade flapping [3]. In other publications, the concentration is found at aggressive maneuvering, trajectory generation and controller design for multiple stages or phases of flight [4]. This information has been further synthesized and advanced in a number of ways in [5]. In [5], the concept of trajectory generation, quadrotor control is applied in various stages of flight to both the single air vehicle case,

as well as team lift applications. In these applications, multiple quadrotors are controlled to move designated objects together and various types of controllers are tuned in order to provide desirable system response characteristics throughout the flight envelope and intended purpose.

The present paper presents a new approach: modeling the coupling dynamics and control of two quadrotors. This new approach presents a host of new issues, which include coupling mechanics and methods, influences of one quadrotor on the other during flight, as well as designing controllers for the new system. We will step through a systematic way of mathematically modeling impact forces, quadrotor equations of motion in both the single and coupled states as well as discuss some other complications that may be important to consider in practical implementation. A magnet-based method of mechanically coupling the quadrotors is proposed. The proposed methods are evaluated through an experiment that involved physical coupling and coupled flight of a pair of quadrotors. The experimental results are presented with a discussion regarding controller gain tuning and system performance characteristics.

The idea of coupled quadrotors presents a new path for many current applications to be extended. It also opens up new avenues that previously have not been considered, such as the pursuit and capture of enemy quadrotors. Also, this idea may extend and improve team lift operations allowing both vehicles to lift a single standard object at the center of gravity, simultaneously improving the inherent stability of the system – a concept that may become more important as the quadrotor begins to be considered as a package delivery platform [6].

The rest of the paper is organized as follows: Section II describes the quadrotors platform and the coupling mechanism. Section III presents the modeling and system dynamics approach of the total system as well as the control architecture for the aforementioned coupling scenarios. Section IV demonstrates the efficiency of the proposed approach through the experimental results. Section V concludes the paper and discusses future work.

## II. QUADROTORS AND COUPLING MECHANISM

Figure 1 shows the quadrotors and the coupling mechanism in our platform. The quadrotor is constructed from lightweight plastic frame with diameter, i.e. the distance between two opposite motors, of 0.25m, and the total weight is approximately 0.55kg. The flight controller is composed of an Ardupilot Mega APM 2.6 controller board<sup>1</sup>, electronic

<sup>1</sup><http://www.ardupilot.co.uk/>

Daniel T. Larsson is with the School of Aerospace Engineering, Georgia Institute of Technology, Atlanta, GA, 30332 USA.

Chuong H. Nguyen was with the School for Engineering of Matter, Transport and Energy, Arizona State University, Tempe, AZ 85287 USA.

Panagiotis Artemiadis is with the Mechanical Engineering Department, at the University of Delaware, Newark, DE 19716, USA.

Email: daniel.larsson@gatech.edu, chuong.h.nguyen@asu.edu, partem@udel.edu

\*Corresponding author: partem@udel.edu

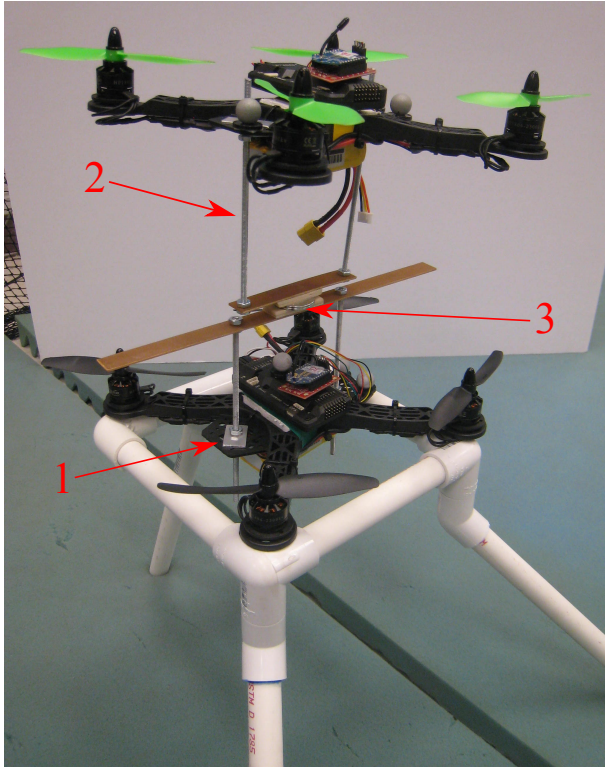


Fig. 1: Quadrotors shown in coupled configuration with coupling mechanism visible.

speed controllers (ESCs), lithium polymer battery and brushless motors with 5 inch(0.127m) diameter propellers. The APM 2.6+ autopilot features a 6 degree of freedom (DOF) inertial measurement unit (IMU) which provides the on-board controllers with vehicle attitude feedback. The autopilot module is connected to the ESCs to control the motor. The quadrotors position are captured via a Vicon motion capture system and sent to the flight vehicles wirelessly via bluetooth from a ground station.

The coupling mechanism is composed of three main components. Referencing Fig. 1, these components are numbered with (1) and (2) being part of the adaptable structure and mounting while (3) shows the location of the magnets. These magnets are approximately 32mm in diameter by 1.6mm thick in size, circular and have a max pull force of approximately 31N [7]. Each quadrotor is outfitted with a single such magnet, mounted directly above (or below) the vehicle center of gravity. This mechanism allows for the quadrotors to couple at arbitrary yaw angles and includes a platform for additional reflective markers to aid in experimentation.

### III. MODELING AND SYSTEM DYNAMICS

#### A. Single Quadrotor Model

Although the dynamics of the quadrotors may be relatively well studied in isolation [3]–[5], a few important distinctions for the case of a coupled system are vital for modeling and designing controller. To facilitate the modeling of a coupled system, we first summarize the dynamics of a single quadrotors in this section.

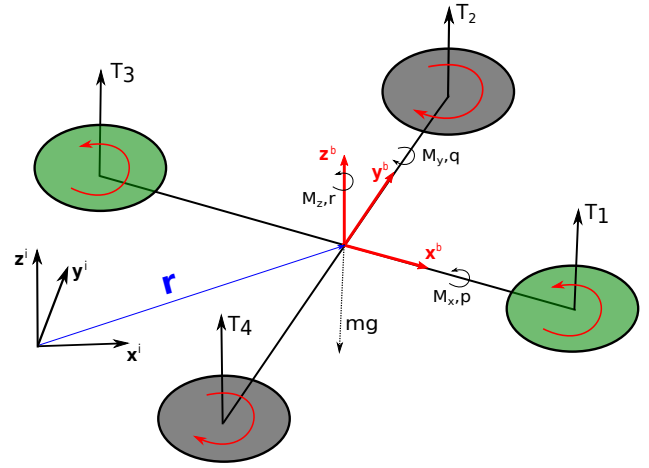


Fig. 2: Free body diagram for the single quadrotor.

Considering the special orthogonal group in three space  $SO(3)$ , and the free body diagram of the quadrotors shown in Fig. 2, let  $\mathbf{F}$  be a vector, e.g. force, position, velocity, in three dimensional space, and  $\mathbf{F}^i = [F_x, F_y, F_z]^i$  and  $\mathbf{F}^b = [F_x, F_y, F_z]^b$  be its coordinate in the inertial frame and the body frame respectively. The set of coordinates are related by:

$$\mathbf{F}^i = \mathbf{R}_b^i \mathbf{F}^b, \quad (1)$$

where  $\mathbf{R}_b^i$  is the rotation matrix:

$$\mathbf{R}_b^i(\omega) = \begin{bmatrix} c_\theta c_\psi & s_\phi s_\theta c_\psi - c_\phi s_\psi & c_\phi s_\theta c_\psi + s_\phi s_\psi \\ c_\theta s_\psi & s_\phi s_\theta s_\psi + c_\phi c_\psi & c_\phi s_\theta s_\psi - s_\phi c_\psi \\ -s_\theta & s_\phi c_\theta & c_\phi c_\theta \end{bmatrix} \quad (2)$$

where  $\omega = [\phi, \theta, \psi]$  are the angular coordinate containing the roll, pitch and yaw angles along  $x, y, z$  axes, respectively while the shorthand notation  $\cos(x) = c_x$  and  $\sin(x) = s_x$  is used. Applying Newton's law to obtain the dynamics in translational motion we have:

$$m\ddot{\mathbf{r}}^i = -\mathbf{P}^i + \mathbf{R}_b^i(\omega)\mathbf{F}_T^b \quad (3)$$

Here,  $\mathbf{r} = [x, y, z]$  is the translation coordinate,  $\mathbf{P}^i = [0, 0, mg]$  is the gravity with the mass  $m$  of the quadrotor,  $\mathbf{F}_T = [0, 0, \sum_{n=1}^4 T_n]$ , where  $T_n$  is the thrust of motor  $n$ . The thrust forces also induce the following moments along the quadrotor body  $x, y, z$  axes:

$$\mathbf{M} = \begin{bmatrix} M_x \\ M_y \\ M_z \end{bmatrix}^b = \begin{bmatrix} l(T_2 - T_4) \\ l(T_3 - T_1) \\ \tau_2 + \tau_4 - \tau_1 - \tau_3 \end{bmatrix}^b \quad (4)$$

where  $l$  is the distance from the center of gravity to the center of any motor.  $\tau_n$  represents the equal and opposite moment applied to the quadrotors due to the torque induced to the propeller shaft. This torque is dependent on the rotational direction of the shaft and is here shown to be consistent with that shown in the free body diagram in Fig. 2.

This moment in turn induces the dynamics in angular motion [4] as

$$\mathbf{I}^b \dot{\nu}^b + \nu^b \times \mathbf{I}^b \nu^b = \mathbf{M} \quad (5)$$

In the above equation,  $\mathbf{I}^b$  is the (approximately) diagonal body-frame inertia tensor matrix,  $\nu^b = [\nu_x, \nu_y, \nu_z]$  are the angular velocities about the body-frame  $x, y, z$  axes. For the specified order of rotations, the corresponding differential equation can be written as [8]:

$$\begin{bmatrix} \nu_x \\ \nu_y \\ \nu_z \end{bmatrix} = \begin{bmatrix} 1 & 0 & -s_\theta \\ 0 & c_\phi & s_\phi c_\theta \\ 0 & -s_\phi & c_\phi c_\theta \end{bmatrix} \begin{bmatrix} \dot{\phi} \\ \dot{\theta} \\ \dot{\psi} \end{bmatrix} \quad (6)$$

The system dynamics are obtained by concatenating the differential equations in (2) - (6).

### B. Dual Quadrotor Coupling Modeling

When the quadrotors are coupled, the dynamics of the system are changed. We assume that the location of the coupled (lower) quadrotor is known with respect to the upper, the coupling mechanism is rigid, and the total system behaves as a rigid body. We also assume that, in the event that the quadrotors were to be coupled at different yaw angles, the relative offset in yaw between the two vehicles is known. In the present study, both flight vehicles are identical, although the analysis is generally formulated and applied to any rigidly connected structure. Considering the free body diagram for the coupled system shown in Fig. 3, the equations of translational motion is similar to (3)

$$m \ddot{\mathbf{r}}^i = -\mathbf{P}^i + \mathbf{R}_b^i(\omega) \mathbf{F}_T^b \quad (7)$$

Here,  $\mathbf{P}^i = [0, 0, m_T g]$  is the gravity with the total mass  $m_T = m_1 + m_2$  of the coupled quadrotors, and  $\mathbf{F}_T = [0, 0, \sum_{n=1}^8 T_n]$ .

In (7), to compute  $\mathbf{R}_b^i(\omega)$ , we can assume that both quadrotors share the same values for roll and pitch angles with a constant offset in yaw angle. This assumption works fine in our simulation. However, as we found in the experiment, this assumption is often violated, as the geometry of the coupling system is not perfectly symmetric, e.g. the centers of gravity of the two quadrotors are not aligned after coupling, and the offset yaw angle slowly drifts. Hence, using roll, pitch, yaw values returned from sensors of either each quadrotors as the representative values for the coupled system will quickly magnify the error in the measured states. These errors will lead to inappropriate control signals, which consequently will cause a severe vibration after coupling and compromise the system's stability.

To overcome this problem, in this preliminary study, we model the system as an inverse pendulum, where each quadrotor is controlled independently similar to the single system described previously, but it also induces an external mass to its counterpart. Thus, the moment applied to the

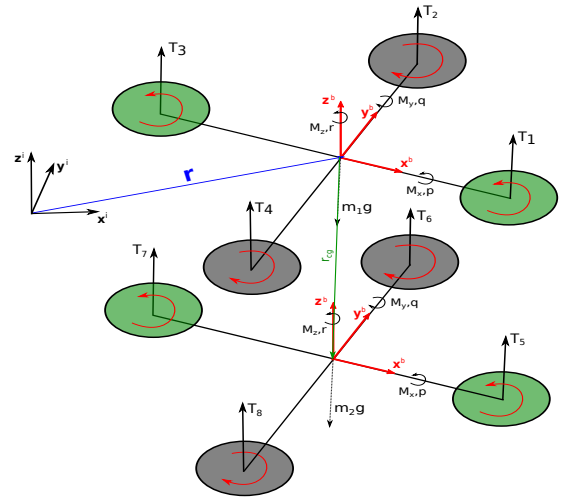


Fig. 3: Free body diagram for the coupled quadrotor system.

upper quadrotor due to the mass of the second can be mathematically expressed using equation (8):

$$\mathbf{M}_2 = \mathbf{r}_{cg}^b \times \mathbf{F}_{cg}^b \quad (8)$$

In the above representation,  $\mathbf{r}_{cg}^b$  is the location of the center of mass of the lower quadrotor expressed in the body frame of the upper. Accordingly,  $\mathbf{F}_{cg}^b$  is the weight vector applied by the lower quadrotor on the upper, in the body frame of the upper. With this in mind,  $\mathbf{F}_{cg}^b$  is defined as:

$$\mathbf{F}_{cg}^b = (\mathbf{R}_b^i)^T \mathbf{F}_{cg}^i, \quad (9)$$

where  $\mathbf{F}_{cg}^i = [0, 0, -m_2 g]$ . Consolidating equations (8) - (9) can be done by utilizing skew-symmetric matrices. In doing so, the following is obtained:

$$\mathbf{M}_2 = [\mathbf{r}_{cg}^b \times] (\mathbf{R}_b^i)^T \mathbf{F}_{cg}^i, \quad (10)$$

Modifying the moment of inertia and accounting for the added motor thrusts, we obtain the complete set of equations describing the rotational dynamics of the coupled system as follows:

$$\mathbf{M}_1 = \begin{bmatrix} l_1(T_2 - T_4) + l_2(T_6 - T_8) \\ l_1(T_3 - T_1) + l_2(T_7 - T_5) \\ \tau_2 + \tau_4 + \tau_6 + \tau_8 - \tau_1 - \tau_3 - \tau_5 - \tau_7 \end{bmatrix}^b \quad (11)$$

where  $\mathbf{M}_1$  is used to denote the applied moment due to differential thrust and  $l_1$  and  $l_2$  are the moment arms of quadrotors one and two, respectively. Then, with  $\mathbf{I}_2^b$  being the body frame moment of inertia of the coupled system, we obtain the final equation below. Equation (12) describes the rotational dynamics of the coupled system:

$$\mathbf{I}_2^b \dot{\nu}^b + \nu^b \times \mathbf{I}_2^b \nu^b = \mathbf{M}_1 + \mathbf{M}_2 \quad (12)$$

Equations (7) - (12) constitute another set of twelve equations describing the nonlinear dynamics of the coupled system.

### C. Controller Methodology - Static Coupling

In this work, we implement a linear quadratic control (LQR) controller [9] combined with PID gain scheduling, as this is a simple, robust and optimal control for under-actuated MIMO systems. Following this approach, we assume that the angles  $\omega = [\phi, \theta, \psi]$  stay in a small region centering at the hover position,  $\omega_0 = [0, 0, \psi_0]$ , i.e.  $|\omega - \omega_0| \leq [10, 10, 10]$  deg. Hence, the nonlinear model of the coupled system can be approximated by a linear model at the operating point  $\omega_0$  as follows

$$\begin{bmatrix} \ddot{x} \\ \ddot{y} \\ \ddot{z} \end{bmatrix} = \begin{bmatrix} g & 0 & 0 \\ 0 & g & 0 \\ 0 & 0 & \frac{1}{m_T} \end{bmatrix} \begin{bmatrix} \theta \cos(\psi) + \phi \sin(\psi) \\ \theta \sin(\psi) - \phi \cos(\psi) \\ \sum_{n=1}^8 T_n - m_T g \end{bmatrix}, \quad (13a)$$

$$\begin{bmatrix} \ddot{\theta} \\ \ddot{\phi} \\ \ddot{\psi} \end{bmatrix} = \begin{bmatrix} \frac{1}{I_x} & 0 & 0 \\ 0 & \frac{1}{I_y} & 0 \\ 0 & 0 & \frac{1}{I_z} \end{bmatrix} (M_1 + M_2) + \delta(t). \quad (13b)$$

where  $\delta(t)$  represents any errors due to the linearization and the disturbance due to the aerodynamic down-wash effect created from the propellers of the top quadrotor acting on the lower.

This system can be divided into two levels. The first level described in (13a) is well modeled and can be controlled easily by the LQR controller. The second level described in (13b) contains all unknown parameters, such as  $\delta_t$ , inertial moments  $I_x, I_y, I_z$ , and the motor dynamics mapping the control voltage  $v$  to the thrust force  $T_n$ . Thus, the PID gain scheduling is implemented as a low level controller.

Specifically, by changing variables

$$B_h = \begin{bmatrix} g & 0 & 0 \\ 0 & g & 0 \\ 0 & 0 & m_T^{-1} \end{bmatrix}, \mathbf{u}_h = \begin{bmatrix} u_x \\ u_y \\ u_z \end{bmatrix} = \begin{bmatrix} \theta \cos(\psi) + \phi \sin(\psi) \\ \theta \sin(\psi) - \phi \cos(\psi) \\ \sum_{n=1}^8 T_n - m_T g \end{bmatrix},$$

the system (13a) can be rewritten as  $\dot{\mathbf{X}} = \mathbf{A}\mathbf{X} + \mathbf{B}\mathbf{u}_h$ ,

$$\mathbf{X} = \begin{bmatrix} \mathbf{r} \\ \dot{\mathbf{r}} \end{bmatrix}, \mathbf{A} = \begin{bmatrix} I_3 & 0_{3 \times 3} \\ 0_{3 \times 3} & 0_{3 \times 3} \end{bmatrix}, \mathbf{B} = \begin{bmatrix} 0_{3 \times 3} \\ \mathbf{B}_h \end{bmatrix},$$

The virtual control signal  $\mathbf{u}_h$  can be obtained by

$$\mathbf{u}_h = \mathbf{K}_{LQR} \mathbf{e}_\rho = \mathbf{K}_P \mathbf{e}_r + \mathbf{K}_I \int_0^T \mathbf{e}_r dt + \mathbf{K}_D \dot{\mathbf{e}}_r$$

where  $\mathbf{e}_r = \mathbf{r}_d - \mathbf{r}$ ,  $\mathbf{e}_{\dot{r}} = \dot{\mathbf{r}}_d - \dot{\mathbf{r}}$ , and the LQR gain  $\mathbf{K}_{LQR} = [\mathbf{K}_P, \mathbf{K}_I, \mathbf{K}_D]$  are obtained by minimizing the following cost function

$$J = \frac{1}{2} \int_0^\infty (\mathbf{e}_\rho^T \mathbf{Q}_m \mathbf{e}_\rho + \mathbf{u}^T \mathbf{R}_m \mathbf{u}) dt \quad (14)$$

In equation (14),  $\mathbf{e}_\rho = [e_r, e_{\dot{r}}, \int_0^T e_r dt]$  is the augmented tracking error,  $\mathbf{u}$  is the desired input and  $\mathbf{Q}_m$  and  $\mathbf{R}_m$  are weighing matrices. The optimal PID gains are obtained by tuning matrices  $\mathbf{Q}_m$  and  $\mathbf{R}_m$  to satisfy desired control performance and authority, i.e. inside the small region centering at the operation points  $\omega_0$  and maximum thrust forces.

TABLE I: LQR gains for High Level controller

Gain	$k_P$	$k_I$	$k_D$	Gain	$k_P$	$k_I$	$k_D$
$K_x$	4.134	2.23	2.882	$K_x$	4.134	2.23	3.6
$K_y$	4.134	2.23	2.882	$K_y$	4.134	2.23	3.6
$K_z$	6.049	3.48	5.0	$K_z$	4.26	1.56 -0	3.6

LQR gains for single mode (left) and coupling mode (right).  $K_{I_z} = 1.56$  for the first quadrotor, and  $K_{I_z} = 0$  for the second.

TABLE II: PID gains for Low Level Controller

Gain	$k_P$	$k_I$	$k_D$	Gain	$k_P$	$k_I$	$k_D$
$K_\theta$	0.4	0.02	0.001	$K_\theta$	0.5	0.025	0.001
$K_\phi$	0.4	0.02	0.001	$K_\phi$	0.5	0.025	0.001
$K_\psi$	0.7	0.04	0.02	$K_\psi$	0.7	0.04	0.02

PID gains for single mode (left) and coupling mode (right)

Deriving the desired roll  $\theta_d$  and pitch  $\phi_d$  and total thrust forces for the low level controller is straight forward as

$$\begin{bmatrix} \theta_d \\ \phi_d \end{bmatrix} = \begin{bmatrix} \cos(\psi) & \sin(\psi) \\ \sin(\psi) & -\cos(\psi) \end{bmatrix}^{-1} \begin{bmatrix} u_x \\ u_z \end{bmatrix}, \quad (15a)$$

$$\begin{bmatrix} u_{T_1} \\ u_{T_2} \end{bmatrix} = \begin{bmatrix} \sum_{n=1}^4 T_n \\ \sum_{n=5}^8 T_n \end{bmatrix} = \begin{bmatrix} \frac{m_1}{m_T} (u_z + m_T g) \\ \frac{m_2}{m_T} (u_z + m_T g) \end{bmatrix}, \quad (15b)$$

The desired values  $\theta_d$  and  $\phi_d$  obtained above and the desired yaw  $\psi_d$  set by user are then sent to the lower level PID control for each quadrotor, to obtain the control signals

$$u_\omega(t) = k_{P,\omega} e_\omega + k_{I,\omega} \int_0^t e_\omega dt + k_{D,\omega} \dot{e}_\omega,$$

where  $e_\omega = \omega_d - \omega$  is the error term, and  $\omega_d = \{\theta_d, \phi_d, \psi_d\}$ . Combined with the thrust force obtained in (15b), the voltage command signal sent to each motor is

$$\begin{bmatrix} vol_1 \\ vol_2 \\ vol_3 \\ vol_4 \end{bmatrix} = \begin{bmatrix} 1 & 1 & 1 & -1 \\ 1 & 1 & -1 & 1 \\ 1 & -1 & 1 & 1 \\ 1 & -1 & -1 & -1 \end{bmatrix} \begin{bmatrix} f_{\text{map}}(u_T) \\ u_\theta \\ u_\phi \\ u_\psi \end{bmatrix},$$

given the motor order specified in Fig. 2, where  $f_{\text{map}}$  is the mapping from thrust force in Newton to the voltage obtained empirically.

## IV. RESULTS

The effectiveness of the proposed coupling mechanism and controller is validated in our experiment, where two quadrotors were autonomously coupled and flown in the new configuration. In the discussion that follows, we refer to the first quadrotor as the upper and the second as the lower.

Figure 4 depicts the progression of the experiment. In phase (A), two quadrotors were initially separated in the inertial space and the first quadrotor flew toward the second one. In phase (B), the first quadrotor landed on the second and they are autonomously coupled before being flown in the coupled configuration depicted in the phase (C). A desired trajectory is designed for both quadrotors before the coupling (independent motion), and after the coupling (joint motion).

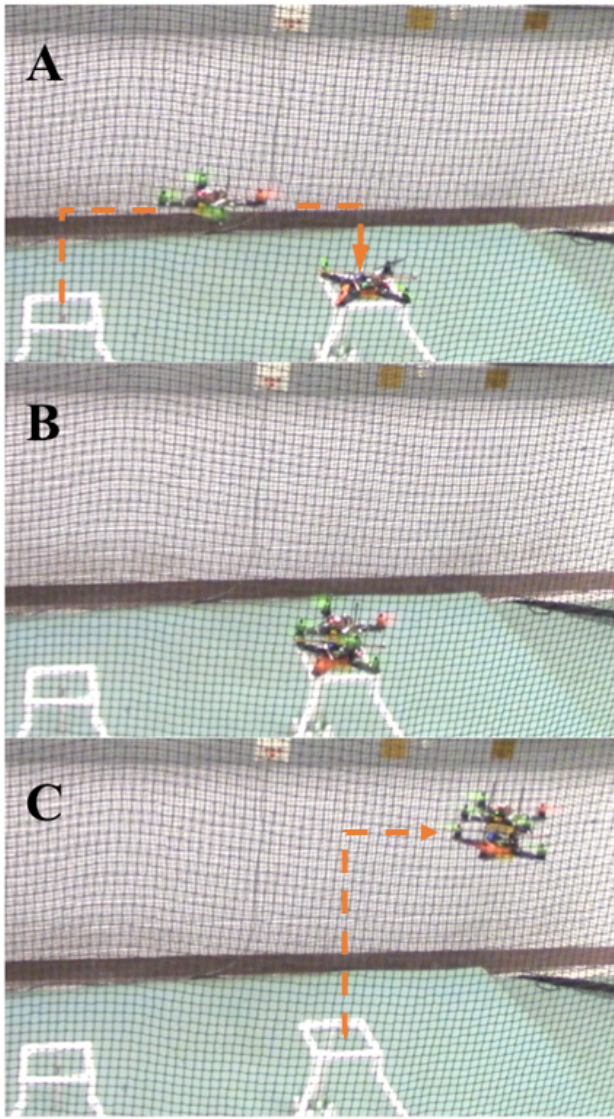


Fig. 4: Experimental progression. (A) quadrotors in pre-coupled configuration, (B) quadrotors during autonomous coupling, and (C) the coupled structure during flight.

The controller gains for two operating modes are given in Table I and II. Comparing between the two modes, we increased the derivative gains in the coupling mode, which corresponds to increase of the damping coefficients of the second order system for  $x$  and  $y$  direction. Hence, the change rate of the desired roll and pitch angles were also reduced. Thus, each low level controller can transiently track the desired signals, so that the difference of the yaw and pitch angles between the two quadrotors remain small, and the coupling mechanism is maintained. The integral gain for tracking  $z$  position of the second quadrotor was also decreased, as the integral term was used to correct any constant offset error. Since the two quadrotors are attached, we only need the first quadrotor to correct this error in order to avoid any possible conflicts between two low level controllers.

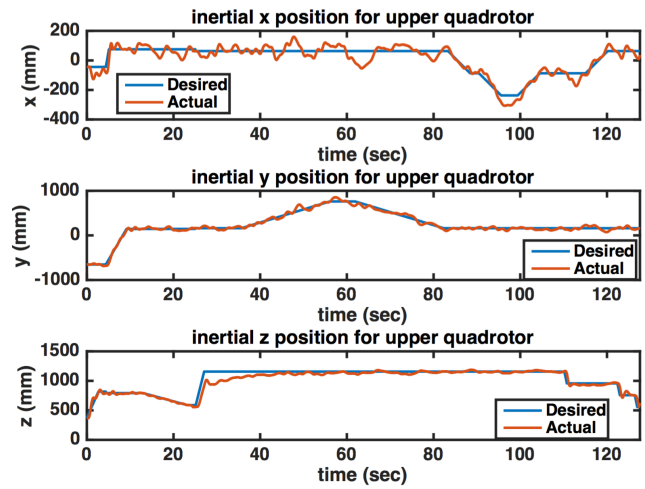


Fig. 5: Experimental results for the upper quadrotor.

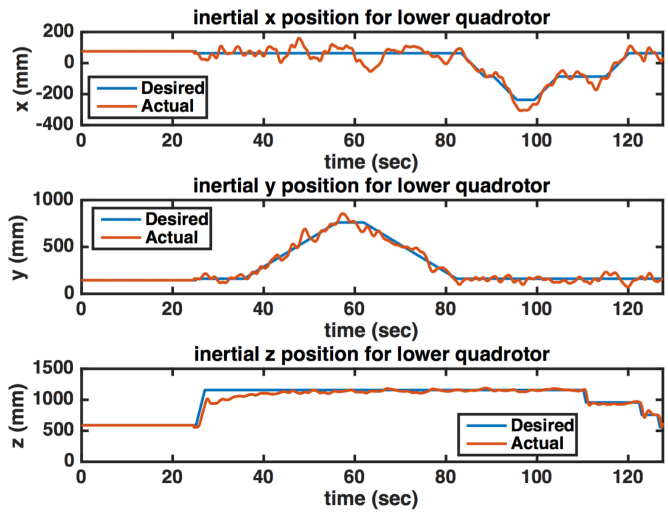


Fig. 6: Experimental results for the lower quadrotor.

Experimental results are shown in Fig. 5 and Fig. 6 while a video of the experiment is available at <https://youtu.be/lZJj5ZGLCFU>. It is seen that the coupled configuration accurately tracks the reference trajectory provided by the ground station in all inertial directions. For the data set presented in Figs. 5 - 6, the quadrotors were coupled at a relative yaw angle of 45 degrees. This was done in order to increase the effective lift of the lower quadrotor and to reduce the aerodynamic disturbance acting on the system. Position feedback obtained from the Vicon motion capture system is used to compute reference attitude inputs to the aerial vehicles. Then, it is the goal of the ground station to appropriately distribute the information to the quadrotors. Additionally, the ground station was also triggering events such as gain scheduling in mid-flight. As shown in Fig. 5 and 6, the tracking error is bounded at 2 - 3cm along each axis, which verifies the high tracking accuracy of the proposed approach.

## V. CONCLUSION

The analysis and evaluation of a coupled quadrotor system opens new frontiers and the possibility of quadrotor rescue, or enemy quadrotor chase and capture. This paper presents the modeling and dynamics of a coupled quadrotor system as well as an experimental results from implementation. Controller gains were found using LQR combined with PID gain scheduling to account for the change in system dynamics to ensure stability and satisfactory response characteristics in actual experiments. Future work will be directed towards the consideration and design of a new coupling mechanism to possibly implement the use of electromagnets or a ball and socket joint in order enable the vehicles to decouple during flight. Furthermore, adaptive control techniques can be incorporated to handle the uncertainty and improve the efficacy of the coupling systems.

## ACKNOWLEDGMENT

This work was supported by the U.S. Defense Advanced Research Projects Agency (DARPA) grant D14AP00068 and U.S. Air Force Office of Scientific Research (AFOSR) awards FA9550-14-1-0149 and FA9550-18-1-0221.

## REFERENCES

- [1] [Online]. Available: <http://www.uavision.com/#!/applications/c1tsl>
- [2] R. Bloss, "Unmanned vehicles while becoming smaller and smarter are addressing new applications in medical, agriculture, in addition to military and security," *Industrial Robot: An International Journal*, vol. 41, pp. 82 – 86, 2014.
- [3] R. Mahony, V. Kumar, and P. Corke, "Multirotor aerial vehicles," *IEEE Robotics & Automation Magazine*, 2012.
- [4] D. Mellinger, N. Michael, and V. Kumar, "Trajectory generation and control for precise aggressive maneuvers with quadrotors," *The International Journal of Robotics Research*, 2012.
- [5] D. W. Mellinger, "Trajectory generation and control for quadrotors," Ph.D. dissertation, University of Pennsylvania, 2012.
- [6] A. Ali, N. Ballou, B. McDougall, and J. L. V. Ramos, "Decision-support tool for designing small package delivery aerial vehicles (dst-spdav)," in *2015 IEEE Systems and Information Engineering Design Symposium*, 2015.
- [7] [Online]. Available: <http://www.kjmagnetics.com/proddetail.asp?prod=DX21>
- [8] B. Etkin and L. D. Reid, *Dynamics of Flight stability and control*, 3rd ed. John Wiley & Sons, 1996.
- [9] K. P. Groves, D. O. Sigthorsson, A. Serrani, S. Yurkovich, M. A. Bolender, and D. B. Doman, "Reference command tracking for a linearized model of an air-breathing hypersonic vehicle," *AIAA Guidance, Navigation, and Control Conference and Exhibit*, 2005.